



Phase behavior of main-chain liquid crystalline polymer networks synthesized by alkyne-azide cycloaddition chemistry

Journal:	<i>Soft Matter</i>
Manuscript ID	SM-ART-09-2018-001913.R2
Article Type:	Paper
Date Submitted by the Author:	09-Nov-2018
Complete List of Authors:	Wang, Yongjian; University of Connecticut, Chemical and Biomolecular Engineering Burke, Kelly; University of Connecticut, Chemical and Biomolecular Engineering; University of Connecticut, Polymer Program, Institute of Materials Science; University of Connecticut, Biomedical Engineering



Journal Name

ARTICLE

Phase behavior of main-chain liquid crystalline polymer networks synthesized by alkyne-azide cycloaddition chemistry

Yongjian Wang^a and Kelly A. Burke^{*a,b,c}Received 00th January 20xx,
Accepted 00th January 20xx

DOI: 10.1039/x0xx00000x

www.rsc.org/

Liquid crystalline polymer networks (LCNs) couple polymer chain organization to molecular ordering, the switching of which has been shown to impart stimuli-responsive properties, including actuation and one-way shape memory, to the networks. While LCNs have long been proposed as artificial muscles, recent reports have also suggested potential as dynamic biomaterial substrates. In contrast to many existing LCNs synthesized using hydrophobic spacers, this work investigates networks synthesized using more hydrophilic spacers to promote interaction with water. A challenge with such materials is liquid crystalline phases could be disrupted in hydrated networks. This work thus investigates the impact of polyether spacers and mesogen composition on the phase behavior of LCNs. Main-chain LCNs were synthesized using alkyne-azide cycloaddition ("Click" chemistry), where two different mesogens (5yH and 5yMe) and a non-LC monomer (5yTe) were coupled with one of two different polyether spacers, poly(ethylene glycol) and poly(propylene glycol), and a crosslinker. The chemistry led to high gel fraction materials, the workup of which resulted in networks that displayed no difference in cellular toxicity due to leachable components compared to tissue culture plastic control. Calorimetric analysis, dynamic mechanical analysis, and X-ray scattering revealed the LC microstructure and temperature-responsive properties of the networks. The use of low molecular weight of the polyether spacers was found to prevent their crystallization within the LC network, and adjusting mesogen composition to enhance its LC phase stability allowed the use of spacers with larger molecular weights and pendant groups. Hydrated networks were found to rearrange their structure compared to dry networks, while maintaining their LC phases. Like other crosslinked LC materials, the networks display shape changes (actuation) that are tied to changes in LC ordering. The result is a new synthetic approach for polydomain networks that form stable LC phases that are tailorable using polyether spacers and may enable future application as hydrated, stimuli-responsive materials.

1. Introduction

Liquid crystalline (LC) polymer networks (LCNs)^{1–3} are crosslinked macromolecules that organize into ordered phases at conditions that are dependent on chemical composition and polymer structure. Ordering induces phase-dependent properties in the network and is driven by molecules called mesogens that can be incorporated directly in the polymer backbone (main-chain LC) or as a pendant group (side-chain LC). In the absence of LC ordering, the networks behave like isotropic networks with properties (e.g. strength and extensibility) that are dependent on crosslink density⁴. Upon formation of an ordered phase, the LCN's mechanical^{5,6,7} and optical^{8,9} properties can be very different than isotropic networks¹⁰, and switching between phases can be repeated without inducing degradation for some compositions. A key LCN behavior enabled by this switching is actuation, which is the

reversible extension and contraction of a LCN when forming liquid crystalline (LC) and isotropic phases, respectively, under applied stress. The stress and stimuli required to induce actuation, as well as the change in dimensions that result, are determined by material design. Actuation was first proposed by de Gennes¹¹, was subsequently demonstrated for both side-chain^{7,12–14} and main-chain LCNs^{15–19}, and has been augmented by experiment, theory, and simulation to reveal design principles^{7,20–22} for actuating networks. More recently, shape changing has been reported in more than one direction, including the bending of films²³ and cantilevers^{24,25}, closure of apertures²⁶, wrinkling²⁷ and other topographical changes^{22,28,29}, and 3D origami³⁰. These more complex shape changes have resulted from advances in methods to control molecular orientation and, in some cases, combining LC materials with other non-actuating materials in novel ways^{30–32}.

Because of the inherent link between molecular scale organization and macroscopic properties, as well as the ability to control mesogen orientation using advanced synthetic and processing techniques^{33–36}, LCNs have been desired for potential applications as valves³⁷, topographical displays^{22,28,29}, and artificial muscles for soft robotics^{7,33,38–44}. More recently, LCNs blended with materials that enable Joule heating for material actuation near 37°C⁴⁵, without requiring significant heating of the surroundings. These materials have been

^a Chemical and Biomolecular Engineering, University of Connecticut, 191 Auditorium Road Unit 3222, Storrs, CT 06269-3222

^b Polymer Program, Institute of Materials Science, University of Connecticut, 97 North Eagleville Road Unit 3136, Storrs, CT 06269-3136

^c Biomedical Engineering, University of Connecticut, 260 Glenbrook Road Unit 3247, Storrs, CT 06269-3247

Electronic Supplementary Information (ESI) available: [details of any supplementary information available should be included here]. See DOI: 10.1039/x0xx00000x

demonstrated compatible with cells for *in vitro* culture, where they are of interest for their ability to stretch and contract like muscle. Other liquid crystal network compositions have also been shown to be compatible with cells^{46–55}, but the cellular compatibility of main-chain polyether-based LCNs prepared using alkyne-azide Click chemistry has not been reported.

One challenge with existing LCN compositions used for culture matrices is that their chemistries are not as readily compatible with reactive groups present on biologically-relevant molecules, such as peptides that are often amine, carboxyl, thiol, *N*-hydroxysuccinimide (NHS), maleimide, or azide-terminated. While not necessary for use as a culture substrate, being able to incorporate protein sequences that assist in cell attachment or enzymatic degradation of the material would allow for functionality that may enhance the relevance of these synthetic substrates. The closest platform that is most readily adapted to incorporate such building blocks are the thiol-alkene (hereafter: thiol-ene) “Click” syntheses^{56–58}. While highly efficient and powerful due to the ability to afford spatial control over polymerization^{59,60}, thiol-ene syntheses require decomposition of the free radical initiator and exposure to either heat or ultraviolet (UV) light. Recent data suggests that careful selection of free radical initiator⁶¹ may be the most important factor to limiting toxicity from radical chemistries. This work sought to investigate an alternative approach: the synthesis of LCNs using alkyne-azide cycloaddition (AAC) chemistry using polyether spacers. The polyether spacers were included for their ability to associate with water, which may facilitate transport of materials in aqueous environments and increase a LCN’s utility in biological applications.

This work reports on the synthesis and characterization of main-chain LCNs using alkyne-azide cycloaddition (AAC) “Click” chemistry, selected for its efficiency and lack of byproduct formation under mild reaction conditions⁶². Click reactions have been conducted at room temperature as well as with or without a catalyst^{63–67}, depending on the solvent and type of alkyne employed. Here, alkyne-terminated mesogens were polymerized with azide-terminated polyether segments to allow some flexibility in the polymer chain. Two polyethers were investigated in this work: poly(ethylene oxide) (PEO) and poly(propylene oxide) (PPO). The length and chemical composition of the polyether segments was varied because it was anticipated that a certain amount of flexibility would be required to promote LC organization, but that too long of a segment may hinder LC phase formation by allowing the polyether to crystallize or providing so much chain entropy that the LC phase would not form successfully. Recent work supports this reasoning, having shown that PEO crystallizes in networks prepared by polymerizing PEO dithiol (molecular weight (Mw) ~1500 Da)⁶⁸ with alkene-terminated mesogens, and that lower molecular PEO dithiol (Mw ~182 Da)⁴⁸ does not crystallize when polymerized with acrylate-terminated mesogens.

All the LCEs in this work were synthesized in dimethylformamide (DMF), at room temperature, and without the need for ultraviolet (UV) light or heating, which may be advantageous for incorporation of more sensitive molecules. Two different LC monomers (mesogens) (**5yH** and **5yMe**) and

one non-LC monomer (**5yTe**) were polymerized with different polyether spacers (PEO and PPO) and a polyether crosslinker to generate networks. The thermal, mechanical, and microstructural properties were characterized to elucidate mesogen organization and phase behavior in these soft networks. This work is synthetically distinct from previous reports of LCNs prepared using polyether spacers in several ways: the synthetic platform used, the compositions of mesogens, and the chemical composition and length of the polyether chain extenders, and the characterization described reveals distinct properties based on these composition differences. Further, the workup developed is a way to reduce the toxicity of the networks and suggests compatibility with cells, though more extensive characterization on this is the subject of current study. Ultimately, this work seeks to lay the synthetic groundwork to a new synthetic platform for LCNs that can be adapted to include biological molecules, which may increase their utility in biological and environmental applications.

2. Experimental

2.1 Reagents.

4-hydroxybenzoic acid (99%), 5-chloro-1-pentyne (98%), hydroquinone (99%), methyl hydroquinone (99%), anhydrous dichloromethane (DCM, 99.8%), 1,3-dicyclohexylcarbodiimide (99%), 4-(dimethylamino)pyridine (99%), potassium hydroxide ($\geq 90\%$), copper(I) bromide (Cu(I)Br, 98%), *N,N*-dimethylformamide (DMF, $\geq 99.9\%$), triethylamine ($\geq 99\%$), anhydrous pyridine (99.8%), 4-pentyn-1-ol (97%), terephthaloyl chloride (99%), anhydrous tetrahydrofuran (THF, $\geq 99.9\%$), sodium bicarbonate ($\geq 99.5\%$), sodium azide (99.5%), poly(propylene oxide) (PPO, Mw~425 Da), deuterated chloroform (CDCl₃, 99.8 atom%D), and ethylenediaminetetraacetic acid (EDTA, $\geq 98.5\%$) were purchased from Millipore Sigma (Burlington, MA). Hydrochloric acid (ACS Plus grade), dichloromethane (DCM, 99.9%), methanol (CH₃OH, 99.9%), hexanes (Certified), 2-propanol (99.9%), glacial acetic acid (Certified ACS Plus), ethyl acetate (99.8%), 6-bromohexanoyl chloride (97%), anhydrous magnesium sulfate (MgSO₄, Certified), Dulbecco's modified eagle medium (DMEM), Neutral Red (pure, high purity biological stain), fetal bovine serum (FBS, qualified), phosphate-buffered saline (PBS, 1x, sterile), and Antibiotic-Antimycotic (anti-anti, 100X) were purchased from Fisher Scientific (Waltham, MA). A tetrafunctional azide-terminated poly(ethylene oxide) (PEO) crosslinker (Mw~2000 Da, referred to here as **PEO-tetraazide**) was purchased from Creative PEGWorks (Chapel Hill, NC). PEO diazide chain extender with Mw~1000 Da (referred to here as **PEO20-diazide**) was purchased from Creative PEGWorks (Chapel Hill, NC). PEO diazide chain extender with Mw~244 Da (referred to here as **PEO3-diazide**) was purchased from BroadPharm (San Diego, CA). Human mesenchymal stem cells (hMSC) derived from bone marrow (Passage 1) were a gift from Prof. David Kaplan of Tufts University and were expanded until use at Passage 5. Ultrapure

water (dH₂O, 18 MOhm.cm) was obtained from an in-house system. Hydroquinone and methyl hydroquinone were purified by recrystallization in toluene (approx. 10g/L) to yield white crystals. Cu(I)Br was purified by washing with glacial acetic acid followed by 2-propanol. DMF was deoxygenated prior to the experiments by nitrogen bubbling for 2-3 h. All the other reagents were used as received.

2.2 Instruments.

Standard differential scanning calorimetry (DSC) experiments were performed on a TA Instruments Q100/Q20 DSC (New Castle, DE). The DSC data was collected by the Q Series Software (version 5.3.0) and analyzed by using the Universal Analysis software (version 4.5A) from TA Instruments (New Castle, DE). Dynamic mechanical analysis (DMA) experiments were performed on a DMA 2980 or a Q800 Dynamic Mechanical Analyzer from TA Instruments (New Castle, DE) with using film tension clamps. The DMA data was collected with Thermal Advantage software (Version 1.1A) and analyzed using the Universal Analysis Software (version 4.5A), both from TA Instruments (New Castle, DE). Confirmation of chemical structures was achieved by liquid phase proton nuclear magnetic resonance (1H NMR) spectroscopy using a Bruker ADVANCE 300 MHz spectrometer and TopSpin 2.1 software, both from Bruker Corporation (Billerica, MA). MestReNova (Version 9.0) software from Mestrelab Research S.L. (Escondido, CA) was used to analyze NMR data. Small-angle X-ray scattering (SAXS) and 2D wide-angle X-ray scattering (WAXS) experiments were performed on a Bruker NanoStar using Cu K α radiation ($\lambda=1.5405$ Å). The data was collected and analyzed using Small Angle X-ray Scattering System software V4.1.45 from Bruker AXS (Billerica, MA). Wide-angle X-ray scattering (WAXS) experiments were performed on an Xcalibur PX Ultra, and data was collected and analyzed using CrysAlisPro (Version 1.171) from Oxford Diffraction (Concord, MA). Voigt peak fitting was used to deconvolute 1D spectrum of WAXS patterns using OriginPro (Version 8.1) from OriginLab (Northampton, MA). The absorbance of the Neutral Red assay at 540 nm was measured using Synergy HT microplate reader and data was collected using Gen5 (Version 1.04.5). Both plate reader and Gen5 are from BioTek Instruments (Winooski, VT).

2.3 Synthesis of Monomers and Chain Extenders.

2.3.1 Synthesis of Monomers. 1,4-phenyl(bis(4-pentyloxybenzoate)) (**5yH**) and (2-methyl-1,4-phenyl(bis(4-pentyloxybenzoate))) (**5yMe**). **5yH**⁶⁹ and **5yMe**^{20,70} are liquid crystalline monomers and were synthesized by modifying a previously published procedure. The method was modified by replacing 5-bromo-1-pentene with 5-chloro-1-pentyne to introduce alkyne functional groups as endgroups on the monomers. **5yMe** was purified by running through a silica gel column (eluent: DCM), and **5yH** was purified by recrystallizing in a mixture of ethyl acetate and 2-propanol (70/30, volumetric ratio). The product of both reactions was a white solid with the structures shown in Figure 1. After purification, the yield of **5yH** was about 60.0% and the yield of **5yMe** was about 55%. 1H NMR

in CDCl₃ gave the following chemical shifts (δ) for **5yH** in ppm: 8.18(4H, m), 7.28(4H, m), 7.02(4H, m), 4.19(4H, t), 2.47(4H, m),

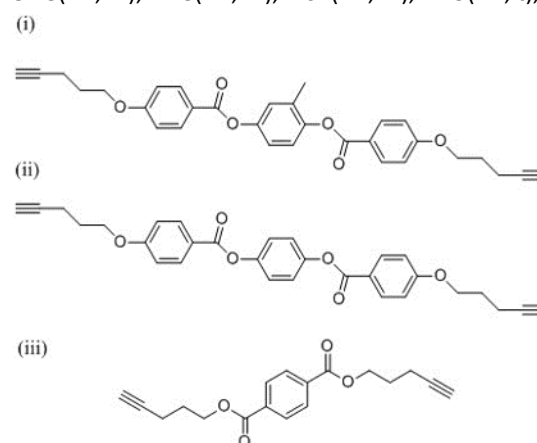


Fig. 1 Structure of monomers: (i) **5yMe**, (ii) **5yH**, and (iii) **5yTe**.

2.07(4H, m), 2.02(2H, t). 1H NMR in CDCl₃ gave the following δ for **5yMe** in ppm: 8.18(4H, m), 7.06-7.23(3H, m), 6.96-7.06(4H, m), 4.19(4H, m), 2.46(4H, m), 2.27(3H, s), 1.98-2.13(6H, m).

1,4-bis(pent-4-ynyl)benzoate (**5yTe**) is a non-liquid crystalline monomer and was synthesized by modifying a method described in literature^{71,72}, where 4-pentyn-1-ol was used instead of 4-penten-1-ol to introduce alkyne functional groups to the monomers. Briefly, 4-pentyn-1-ol, terephthaloyl chloride, and pyridine were added into THF to react for 4h at 70°C, then the products were purified by extraction and washing. The product was white solid with yields typical of the literature. 1H NMR in CDCl₃ gave the following δ in ppm: 8.12(4H, s), 4.48(4H, t), 2.42(4H, m), 2.10-1.98(6H, m).

2.3.2 Synthesis of Chain Extenders. Poly(propylene glycol) Bis-6-azidohexanoate (**PPO7-diazide** chain extender) was synthesized by modifying a procedure from literature to accommodate a lower molecular weight PPO chain as the starting material⁷³. Briefly, the hydroxyl-terminated PPO was modified using 6-bromohexanoyl chloride to be bromo-terminated. Sodium azide was subsequently used to replace bromine with azide. The product was purified by extraction and washing. The product was clear oil and yield was about 58.3%. 1H NMR in CDCl₃ gave the following δ in ppm: 3.75-3.10(24H, m), 2.51-2.24(3H, m), 1.71-1.56(8H, m), 1.48-1.33(4H, m), 1.27-1.07(21H, m). The other two chain extenders, **PEO3-diazide** and **PEO20-diazide**, were purchased and used as received (see Reagents).

2.4 Synthesis of Liquid Crystalline Networks using Alkyne-Azide Cycloaddition.

The liquid crystalline (LC) and non-liquid crystalline networks were synthesized by reacting the alkyne monomers (LC monomers: **5yMe** and **5yH**; non-LC monomer: **5yTe**) with the diazide chain extenders (**PEO3-azide**, **PEO20-azide**, or **PPO7-azide**) and the **PEO-tetraazide** crosslinker. Networks are named using the following convention: **N-monomer_{moles}-chain extender_{moles}**, where the prefix **N-** denotes a crosslinked network and the subscript denotes the number of moles of that

component relative to one mole of **PEO-tetraazide** crosslinker in the reacting solution. As an example, **N-5yMe₆-PEO3₄** was synthesized using six moles of **5yMe** and four moles of **PEO3-diazide** per one mole of **PEO-tetraazide** crosslinker.

All networks were synthesized using the same concentration of reagents and catalysts in DMF, hence the synthesis of **N-5yMe₆-PEO3₄** is described as a representative example. **5yMe** (63.54 mg, 0.1281 mmol) was weighed into a 25 mL Schlenk flask and purged with nitrogen gas for 2 min. Deoxygenated DMF (0.35 mL) was added to the flask to dissolve the mesogen. After dissolution, the vessel was quickly opened to add the **PEO3-azide** (0.0854 mmol, 20 μ L). The vessel was then purged to remove oxygen, and the mixture was stirred until the **PEO3-azide** dissolved. **PEO-tetraazide** (0.02135 mmol, 73 μ L) was added to the flask the same way. Cu(I)Br (10 mg, 0.07 mmol) was then dissolved in 0.15 mL deoxygenated DMF, which was subsequently injected through a septum and into the flask. The reacting mixture was purged for 3 min before transferring to a mold consisting of two glass slides separated by a polytetrafluoroethylene spacer (mold area: 65.0 mm length x 18.0 mm width x 300 μ m thickness). The solution was allowed to react at room temperature for 24 h. Samples were demolded and vacuum dried at 60°C overnight to result in a crosslinked film.

2.5 Removal of Copper Catalyst and Extraction of Soluble Polymer.

All networks were extracted three times for 6h each using DMF, and then extracted three times for 6h each using 0.1M EDTA/H₂O solution to remove copper catalyst. The networks were weighed before and after extraction, and network gel fraction was calculated by dividing the post-extraction mass by the pre-extraction mass.

2.6 Characterization Methods.

To measure thermal transitions, monomers and films were encapsulated within aluminium pans for Differential Scanning Calorimetry (DSC). Samples were subjected to the following thermal program: cool to -80°C, hold for 2 min, heat to the isotropic phase at 10°C/min, hold for 2 min, cool once again to -80°C at 10°C/min, and hold for 2 min. The cycle was then repeated, and the second heating and cooling traces were studied to compare samples with uniform thermal history. POM samples were prepared by drop casting a solution of monomer (1% in DCM) onto clean glass coverslips and allowing it to dry in a fume hood. Samples were then heated to the isotropic, held for 5 min, and then cooled back to -20°C at 10°C/min using the microscope's heating/cooling stage. Images were acquired with during the second heating and cooling traces, the rate of each was 10°C/min to match the rate of DSC.

Storage modulus and loss modulus were measured as a function of temperature using a Dynamic Mechanical Analyzer (DMA). Films (typical size: 10 mm length x 2.0 mm width x 0.2 mm thickness) were mounted in the instrument, and the samples were oscillated at a prescribed amplitude (10 μ m) and frequency (1 Hz) while heating from -70°C to 150°C at 3°C/min. Two-way shape memory (actuation cycles) were also performed on a DMA by operating the instrument in controlled force mode. For these experiments, films were loaded into the tensile

clamps and heated to the isotropic phase before a static load was applied. The film was then cooled under constant load to -60°C and held for a brief isothermal (5 min) before heating back to the isotropic phase. Both heating and cooling rates were 3°C/min. The load was increased for subsequent cycles.

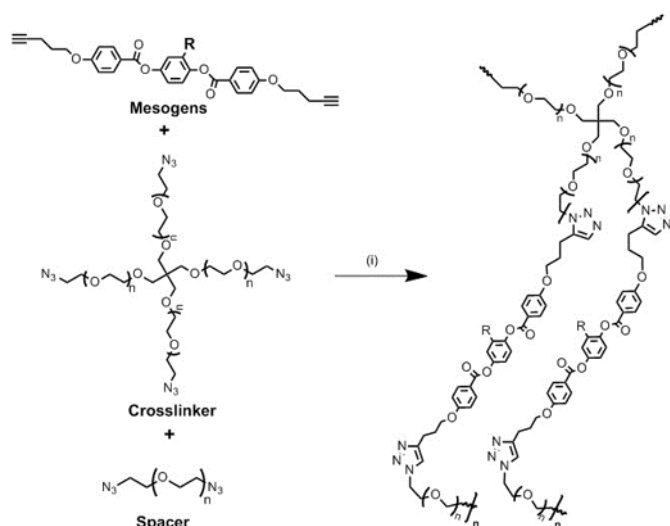
Wide-Angle X-ray Scattering (WAXS) and Small-Angle X-ray Scattering (SAXS) were both performed at room temperature on samples that were previously heated to the isotropic and cooled back to room temperature to erase thermal history. Exposure times were 30 minutes for dry samples and one hour for hydrated samples. For SAXS acquired at different temperatures, samples were heated to the temperature of interest at 5°C/min and held for 10 min to ensure temperature uniformity before acquiring the data.

A Neutral Red assay was used to quantify cytotoxicity⁷⁴ of the extracted networks. Films of LC and non-LC networks (size: 10 mm length x 10 mm width x 0.2 mm thickness) were sterilized by soaking in 70% ethanol overnight and were then washed three times using sterile PBS. After washing and drying, each sample was soaked in 0.24 mL complete medium (89% DMEM, 10% FBS, and 1% anti-anti) for 72 hours in a sterile 48-well plate (Plate 1) to allow leachable materials to enter the medium. Human mesenchymal stem cells (hMSCs, P5) were seeded onto a second 48-well plate (Plate 2) at 15,000 cells/cm² for the experimental and control groups. Separate wells containing varying amounts of hMSCs were also seeded for a standard curve. The cells were incubated (37°C, 5% CO₂) in fresh complete medium overnight prior to the start of the assay. Medium, which had been soaking with the networks (experimental group) or the tissue culture plate (positive control for viability) for 72 hours, was then transferred from Plate 1 to Plate 2. Medium containing Triton X-100 was added to separate wells for a negative control for cell viability. The cells were returned to the incubator and after 24 hours, 0.12 mL of a Neutral Red stock solution (4 mg/ml in PBS) was added into 12 mL complete medium to make a Neutral Red working solution. Cells were stained with the working solution for three hours at 37°C and 5% CO₂. The working solution was then removed, and the wells were washed with PBS three times to remove residual stain. Cells were destained at room temperature by adding 0.19 mL/well destaining solution (5 mL deionized water, 5 mL ethanol, and 0.1 mL acetic acid) and applying gentle rocking for 10 minutes. The supernatant was transferred to a 96 well plate to measure the absorbance of Neutral Red at 540 nm, where higher values indicated the presence of more live cells. Means and standard deviations of replicates are reported. One-way analysis of a variance (ANOVA) with a Holm-Sidak Post-test was used to generate comparisons between groups. Significance was determined at a level of $\alpha = 0.05$.

3. Results and discussion

3.1 Synthesis of Networks.

The synthesis of liquid crystalline networks (LCNs) is shown in Scheme 1. Non-liquid crystalline networks were prepared similarly, except the non-LC monomer, **5yTe**, was used in place



Scheme 1. Scheme of LC network synthesis using mesogens, **PEO-diazide** spacers, and **a PEO-tetraazide** crosslinker by click coupling. (i) CuBr, DMF, 25°C. R=H for **5yH** and R=CH₃ for **5yMe**.

of the LC monomers (**5yH** or **5yMe**). All components were dissolved in deoxygenated DMF, and the homogeneous solution was injected into a two-part glass mold to provide uniform film thickness. The crosslinked film was demolded after reacting 24h at room temperature. All films were extracted, as described in the Experimental Section, prior to analysis to remove any soluble components. Gel fraction was measured in triplicate and always exceeded 85.0%, indicating successful network formation. No alignment technique was applied to the films, thus the LC networks are polydomain. Visual inspection shows all LC films are translucent, and that the non-LC films are transparent. LC domains are expected to be at least 400 nm in size because of their ability to scatter light, though this was not quantified with scattering equipment.

3.2 Phase Behavior of Monomers.

Differential scanning calorimetry (DSC) and Polarized Optical Microscopy (POM) were used to detect transitions of the liquid crystalline monomers. Two monomers were investigated to provide opportunity for tailoring of LC phase stability in the dry and hydrated states. The thermal transitions of **5yMe** and **5yH** were studied using DSC, and their second heating traces and cooling traces (both 10°C/min) are shown in Supplementary Information (SI) (Figure S1). POM images, shown in SI Figure S2, were acquired upon cooling the samples from the isotropic to -20°C at 10°C/min for **5yMe** and **5yH**. Upon cooling from the isotropic, birefringence was observed with threaded nematic LC texture. Further cooling resulted in crystallization of the monomer, as indicated by a birefringent “feather-like” crystal. These transitions were consistent with the transitions observed in the DSC (Fig. S1). The temperatures and latent heat values for each transition are summarized in Table 1. Switching the substitution on the mesogen’s central aromatic ring from a methyl group to a hydrogen was found to increase the isotropization temperature and to increase the crystalline content of the monomer. These results are consistent with

Table 1 Temperatures of crystallization (cry), recrystallization (recry), melting (melt), isotropization (iso), and anisotropization (aniso) for **5yH** and **5yMe** monomers, as measured by DSC. Latent heats of each transition located in parentheses.

	T _{recry} , °C (ΔH, J/g) (heating)	T _{cry} , °C (ΔH, J/g) (cooling)	T _{melt} , °C (ΔH, J/g) (heating)	T _{iso} , °C (ΔH, J/g) (heating)	T _{aniso} , °C (ΔH, J/g) (cooling)
5yH	65.0 (10.4)	76.1 (63.4)	123 (95.3)	227 (3.99)	226 (3.49)
5yMe	21.9 (1.48)	50.0 (60.4)	133 (86.8)	172 (3.65)	171 (3.54)

literature trends^{69,75–78} that increasing the bulkiness of lateral substitutions on mesogens can reduce the propensity of the molecule to crystallize and the stability of its liquid crystalline mesophase. Additionally, both mesogens show similar phase behaviour to previously reported alkene-terminated mesogens^{69,70}.

3.3 Thermomechanical Characterization of Networks.

This section describes the impact of mesogen and polyether chain extender composition on the phase behavior and transitions of crosslinked networks. Specifically, chain extenders were varied to produce networks that favor strong LC phase formation, even when hydrated, and that do not result in chain extender crystallization. Mesogens were varied because tuning their ability to organize enables the synthesis of networks that display liquid crystallinity using different chain extenders, including extenders with pendant groups (PPO) and larger molecular weights (PEO). DSC data is discussed first and is followed by DMA data. Networks are named by their composition using the convention noted previously, where the prefix **N-** denotes a crosslinked network and the subscript denotes the number of moles of that component relative to one mole of **PEO-tetraazide** crosslinker. As an example, **N-5yH₆-PPO7₄** was synthesized using six moles of **5yH** and four moles of **PEO-diazide** per one mole of **PEO-tetraazide** crosslinker.

Figure 2 shows representative second heating traces acquired using DSC of networks prepared from **5yMe** (Fig. 2a) and **5yH** (Fig. 2b). All networks analyzed (Fig. 2a, 2b, and SI Fig. S3 for **5yTe**-based networks) showed stepwise decrease in the second heating traces around -37°C to -25°C, which is attributed to the glass transition of the network. Neither of the compositions shown for **5yMe-PEO3** networks show an endotherm associated with the LC to isotropic transition in the second heating trace, though one was observed in the first heating trace (see Supplementary Information, Fig S4). This suggests that LC ordering in the **5yMe** networks is either too weak to detect using standard DSC or that the ordering may require additional time to develop in these compositions. Mechanical testing and WAXS both suggest that these materials do form LC phases, as shown later. Neither **N-5yMe₆-PEO20₄** (Fig 2a, trace iii) nor **N-5yMe₆-PPO7₄** (Supplementary Info, Fig S5) form LC phases that are detectable using DSC or dynamic mechanical analysis. The loss of LC structure in **5yMe-PEO20** and **5yMe-PPO7** networks may be due to the higher molecular

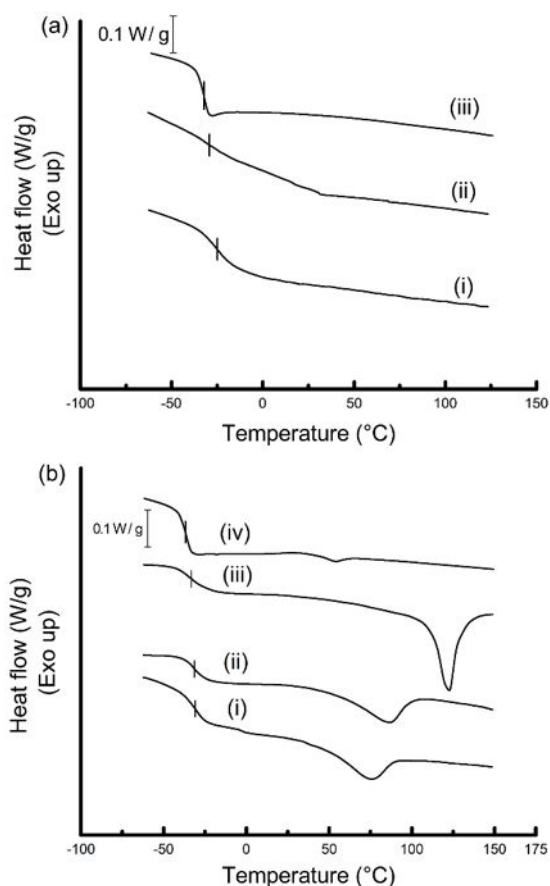


Fig. 2 (a) Second heating DSC traces of **5yMe** network films: (i) **N-5yMe₆-PEO₃₄**, (ii) **N-5yMe₁₂-PEO₃₁₀**, and (iii) **N-5yMe₆-PEO₂₀₄** (b) Second heating DSC traces of **5yH** network films: (i) **N-5yH₆-PPO₇₄**, (ii) **N-5yH₁₂-PPO₇₁₀**, (iii) **N-5yH₆-PEO₃₄**, and (iv) **N-5yH₆-PEO₂₀₄**.

weight of the polyether spacers and/or the weaker interaction strength between **5yMe** mesogens compared to the **5yH** mesogens. The kinetics of LC phase development in those materials are currently under investigation.

In contrast to **5yMe** networks, the DSC results from **5yH** networks show endothermic transitions at higher temperatures than the glass transition (T_g is around -37 to -30°C for all **5yH** networks) in the second heating trace (Fig 2b, traces i-iv). These endotherms are located between 53°C and 122°C . Due to the fact that these temperatures are well above the crystallization temperature of PEO, and the fact that PPO does not crystallize, these transitions are attributed to LC ordering within the network. This conclusion is further supported by analysis of latent heats of the transitions, thermomechanical properties, and microstructure analysis of the networks. Comparing the effect of chain extender (**PEO3** vs. **PPO7** vs. **PEO20**) in the **5yH** networks, the endotherm of **N-5yH₆-PEO₃₄** (Fig. 2b, trace iii) was located at the highest temperature, 122°C , and had the largest latent heat of the transition, $\Delta H = 12.7$ J/g. The endotherms of **5yH-PPO** networks (Fig. 2b, traces i and ii), regardless of crosslink density tested, displayed both lower temperatures and latent heats for this transition. It was found that endotherm of **N-5yH₆-PEO₂₀₄** (Fig. 2b, trace iv) was located

at the lowest temperature, 53°C , and had the smallest latent heat in of all of the **5yH** networks.

Comparing **PEO3**-based networks with **PEO20**-based networks, the results suggest that different numbers of repeat units can reduce LC phase stability, indicating more repeat units (higher molecular weights) can promote chain flexibility and dilute mesogen content in the networks. These results also indicate that the **PPO7**-based networks display less stable LC phases than the **PEO3**-based networks. It should be noted that, because the **PPO7** and **PEO3** chain extenders contain different numbers of repeat units, these studies cannot determine if the destabilization of the LC phase in the **PPO7** materials are due to more repeat units in this extender or because this extender has a methyl side chain, which may hinder chain rotations and disrupt backbone associations to reduce LC phase stability. It is anticipated that both contribute, however this is a limitation in commercially-available reagents and would therefore require custom synthesis for tight control over number of repeat units to elucidate why LC phases are disrupted in **PPO7**-based networks. It should further be noted that no evidence of **PEO3**, **PPO7** or **PEO20** crystallization was observed in the DSC, DMA, or X-ray results of materials presented in this manuscript.

The thermomechanical properties of LC networks were characterized using a dynamic mechanical analyzer (DMA) operated in tensile mode. Figure 3a shows the results from DMA testing of **PEO3**-based networks prepared with different monomers (**5yH**, **5yMe**, and **5yTe**) at constant crosslink density, and Figure 3b shows DMA results from **5yH**-based networks prepared with different spacers (**PEO3**, **PPO7**, and **PEO20**) where the molar ratio of reactants remained constant. The DMA results from **PEO3** and **PPO7**-based networks prepared at different crosslink densities using **5yMe** are shown in Supplementary Information (Figure S6). The storage modulus of all the films showed a dramatic stepwise decrease from -30°C to 30°C . In all of the films, the step starts around -30 to -25°C and its initiation is independent of mesogen and chain extender composition, which suggests that this is due to a glass transition.

Comparing the non-LC network (**N-5yTe₆-PEO₃₄**) to the LC networks in Fig. 3a, the first stepwise decrease in storage modulus for all of the LC networks is broader and displays a shoulder on the higher temperature side of the transition (around 15°C). This transition has also been observed in the DMA traces of other LC materials containing polyether spacers^{68,79}, though it has not yet been ascribed to a specific material property or transition. In addition to being observable in the DMA data, a shift in the SAXS patterns is also observable around the same temperatures. Selected linear polymers were synthesized and studied using DSC, where it was found that linear LC polymers had a glass transition around room temperature, but the non-LC polymer's glass transition was -20°C (see SI Fig. S7). These linear polymers were prepared to gain an expectation of trends only, as literature shows that transition temperatures measured by DSC and DMA may not exactly match. The DMA data shown in Figure 3 are for crosslinked networks, therefore the LCN's broad decrease in storage modulus may arise from different lengths of polymer

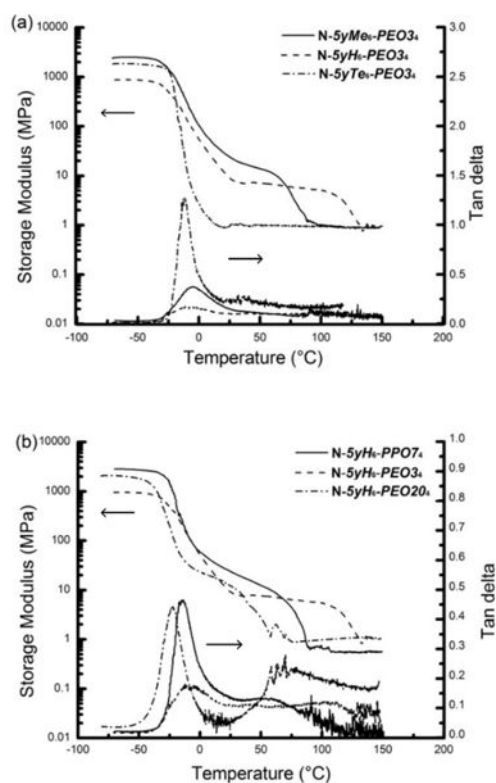


Fig. 3 (a) Tensile storage modulus and tan delta as a function of temperature for LCNs synthesized with different mesogens. (b) Tensile storage modulus and tan delta as a function of temperature for **5yH**-based networks synthesized with different spacers.

chains between crosslinking points. Other possibilities may also explain the transition, such as small scale phase separation. Both of these could increase network heterogeneity, which can result in a distribution of glass transition temperatures and the observation of a broadened transition.

All films that contain mesogen show a second stepwise decrease in storage modulus at a higher temperature than the first transition (Fig. 3a and 3b). The step is consistent with the endotherm observed in the second heating DSC trace and is located at higher temperatures (50°C to 125°C) than would be associated with crystallization⁸⁰ of chain extender or crosslinker. Networks prepared with the non-LC monomer, **5yTe** (**N-5yTe₆-PEO₃** shown in Fig. 3a; **N-5yTe₆-PPO₇** shown in SI Fig. S8), lack this transition. This transition is thus attributed to the change in LC ordering and is the isotropization transition (T_{LC-I}), where mesogens are organized into a LC phase below the T_{LC-I} but are isotropic above this transition. The stepwise decrease in storage modulus upon passing through the isotropization transition has been demonstrated for many other LC network compositions (see Refs. 22 and 48 as examples).

LC networks with different mesogens are compared in Figure 3a. Unlike DSC data, the isotropization transition can be observed using DMA for **N-5yMe₆-PEO₃**, which suggests that DMA measurements are more sensitive for detecting network isotropization, a finding that is consistent with siloxane-based LC elastomers prepared using a mesogen with similar structure

to **5yMe²⁰**. **N-5yH₆-PEO₃** displays a higher T_{LC-I} than **N-5yMe₆-PEO₃** because **5yH** forms more stable LC phases than **5yMe**. As long as the network is liquid crystalline, this trend was observed when controlling for chain extender and crosslink density. The stepwise transition temperature initiated around -30 to -25°C is not affected by the change in mesogen and also appears in non-liquid crystalline **5yTe**-networks, both of which supports that this transition is due to a glass transition (T_g).

The DMA results of LC networks prepared using **5yH** and different chain extenders are shown in Figure 3b. Two strong stepwise decreases in the storage modulus signal can be observed for all **5yH** networks. The decrease in storage modulus at higher temperature indicates isotropization of **5yH** networks, and the broad decrease at lower temperature is attributed to the glass transition. Comparing the three different chain extenders, **N-5yH₆-PEO₂₀** shows the lowest isotropization temperature in **5yH** networks, suggesting again that the **PEO₂₀** spacer results in the formation of the weakest LC phase compared to the networks formed with the **PEO₃** and **PPO₇** spacers, a finding that is consistent with DSC results. Finally, LC networks with different crosslink density were prepared (shown in Supplementary Information Figure S6). For **5yMe** networks, it is noted that a strong stepwise decrease in storage modulus at 90°C was observed for **N-5yMe₆-PEO₃**, but this transition is weaker in **N-5yMe₁₂-PEO₃**. This difficulty in detecting a strong signal of isotropization in DMA for **N-5yMe₁₂-PEO₃**, the lowest crosslink density material studied here, suggests that the increase in chain mobility supersedes the increase in concentration of mesogens relative to crosslinker content in **5yMe**-based networks. Despite difficulty detecting isotropization using the DMA, **N-5yMe₁₂-PEO₃** is thought to form liquid crystalline phases because mesogen ordering was observed in X-ray scattering data and the material does display thermomechanical actuation behavior. In contrast, over the range of crosslink densities studied, all **5yH** networks displayed strong LC phases (Supplementary Information Fig. S6). Decreasing crosslinker density was found to slightly increase T_{LC-I} without a measurable change in the glass transition. The increase in T_{LC-I} with decreasing crosslink density indicates that the LC phase is more stable, which may be due to two factors. The first is the reduction in the constraints on the polymer chain that can permit mesogens to more readily order, and the second is the increased mesogen concentration in the network.

Table 2 summarizes the transition temperatures from DSC and DMA. In DMA, both the glass transition and the isotropization transition were determined from the position of

Table 2 Glass transition temperature and isotropization temperature (T_{LC-I}) of LCNs measured by DSC and DMA.

	T_g , °C		T_{LC-I} , °C	
	From DSC	From DMA	From DSC	From DMA
N-5yMe₆-PEO₃	-25.1	-9.81	Not Obs.	90.2
N-5yMe₁₂-PEO₃	-31.2	-13.3	Not Obs.	98.2
N-5yH₆-PEO₃	-33.1	-11.6	123	130
N-5yH₆-PPO₇	-30.2	-13.9	75.0	91.0
N-5yH₁₂-PPO₇	-31.4	-11.5	85.9	93.1

the peak in the tan delta trace. In DSC, both transitions were determined from the heating trace, where the glass transition temperature corresponds to the midpoint of the stepwise change in heat flow and the isotropization temperature corresponds to the minimum of the endothermic peak.

3.4 Actuation of Networks

Consistent with other liquid crystalline networks, the polyether LCNs were found to display thermomechanical actuation (two-way shape memory) around their order-disorder transition (Figure 4). Both chemically crosslinked semicrystalline and liquid crystalline networks have been shown to increase in length upon cooling through the crystallization (T_c) temperature and the isotropic-to-LC (T_{I-LC}) transition temperature, respectively. This behavior is reversible, thus contraction of the film occurs upon heating. In semicrystalline materials, this behavior^{81,82} has been attributed⁸² to crystallization along the strain axis. In nematic and smectic LC materials this has been attributed to distortion of the polymer chains away from a spherical-like conformation in the isotropic to an elliptical-like conformation due to the ordering of the LC phase⁸³. In this work, actuation could arise due to liquid crystallinity or crystallization of PEO, but the onset temperatures for these should be very different because T_{I-LC} occurs at higher temperatures upon cooling than the crystallization of PEO. Similarly, the contraction upon becoming isotropic at T_{LC-I} should occur at higher temperatures than the melting transition (T_m) of PEO. PPO is not expected to crystallize

and therefore any shape change in those materials is expected to arise from changes in mesogen ordering.

Strain versus temperature plots for the actuation experiments are shown in Figure 4 for **N-5yMe₆-PEO₃₄** (Fig. 4a), **N-5yH₆-PEO₃₄** (Fig. 4b), **N-5yH₆-PPO₇₄** (Fig. 4c), and **N-5yH₁₂-PEO₃₁₀** (Fig. 4d). All networks display actuation behavior, as evidenced by an elongation in the network upon cooling the film from the isotropic to an LC phase under constant load. As stress increases, the strain evolved during the actuation cycle increases for all networks (Fig 4a-d), a finding that is consistent with the literature. For all **5yH** networks (Fig 4b-d) and **N-5yMe₁₂-PEO₃₁₀** (shown in Supplementary Information Fig. S9), the temperature at which the shape change occurs (temperature at half actuation on heating trace), here termed the actuation temperature, is similar to the T_{LC-I} identified using DSC and the dynamic DMA experiments. A duplicate figure of Figure 4 with half-actuation temperature marked on the curves is provided in Supplementary Information (Figure S10). The half-actuation temperature and breadth between heating and cooling trace at half actuation are shown in Table 3 for films cycled under 75 kPa stress. It should be noticed that breadth of **5yH-PEO₃** is the smallest of the **5yH** networks, suggesting that it has the quickest induction of LC structure on cooling from the isotropic due to its strong liquid crystalline phase. Compared to previous reports of other LCNs, these transitions are relatively broad and this is attributed to high crosslink density, which can hinder mesogen ordering, and the polydomain structure of the networks that

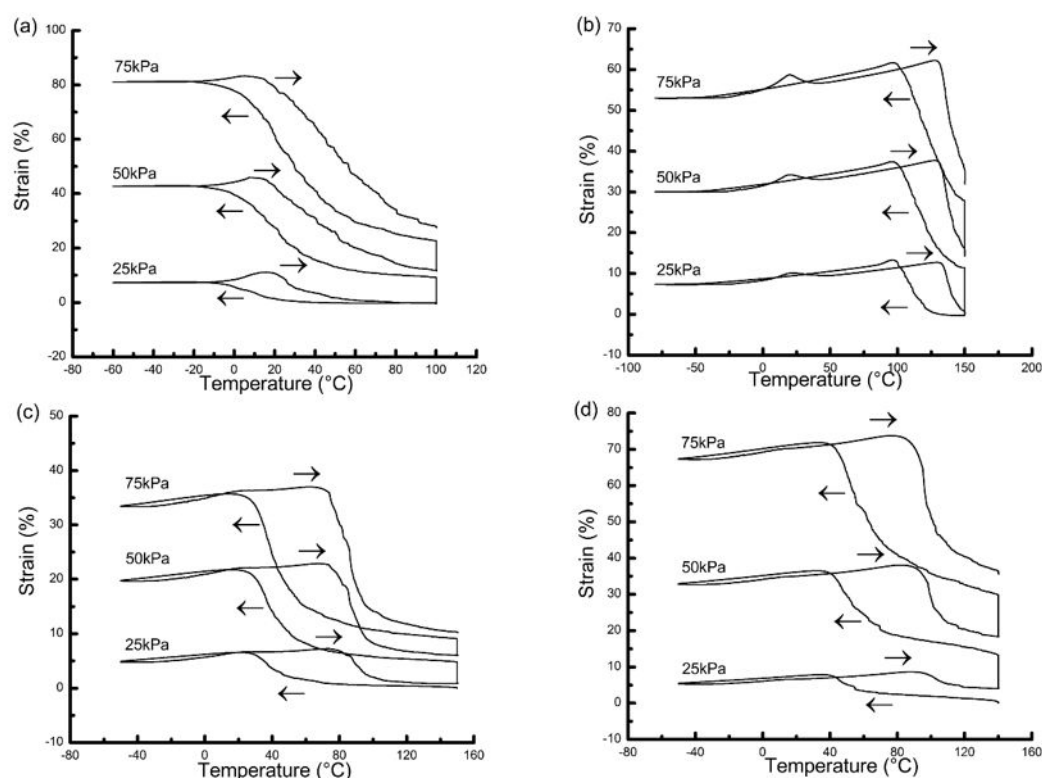


Fig. 4 Actuation (two-way shape memory cycles) of LCNs measured by DMA in controlled force mode. (a) **N-5yMe₆-PEO₃₄** (b) **N-5yH₆-PEO₃₄** (c) **N-5yH₆-PPO₇₄** (d) **N-5yH₁₂-PEO₃₁₀**

Table 3 Comparison of transition temperatures for 75 kPa actuation cycle. The temperatures where the sample reached half of its maximum actuation strain on the heating and cooling cycles are shown. The breadth of the transition is the difference between those temperatures.

	Temperature at Half Actuation Strain (°C) (heating)	Temperature at Half Actuation Strain (°C) (cooling)	Breadth of Transition (°C)
N-5yMe₆-PEO₃₄	53.4	29.0	24.4
N-5yH₆-PEO₃₄	140.	121	18.9
N-5yH₆-PPO₇₄	86.5	41.9	44.6
N-5yH₁₂-PPO₇₁₀	98.5	59.5	39.0

will display smaller actuation strains compared to monodomain networks. In contrast, the actuation temperature of **N-5yMe₆-PEO₃₄** (Fig. 4a) is around 30°C, which does not correspond to the T_{LC-I} of this material. The shape change during actuation of **N-5yMe₆-PEO₃₄** is more closely associated with the broadened stepwise transition, suggesting that it may be associated with relaxation of LC polymer chains or the crystallization of **PEO₃** due to stretching, rather than liquid crystalline organization. At minimum, the low ordering of **N-5yMe₆-PEO₃₄** results in a wide temperature range needed for actuation to occur, which may limit the material's utility as a shape changing material. It should be noted that **N-5yMe₆-PEO₃₄** could be investigated further using WAXS in concert with film stretching to elucidate how LC ordering and polymer crystallization change during the actuation cycle, however this was not possible at the time of these studies.

3.5 Microstructural Characterization of Networks

The unique thermomechanical properties of LCNs are attributed to liquid crystalline microstructure, which was characterized by X-ray scattering. A series of non-liquid crystalline networks were first synthesized by reacting the non-LC monomer, **5yTe**, with **PEO₃** or **PPO₇** chain extenders and crosslinking with **PEO-tetraazide** to establish the structure of isotropic networks. 2D WAXS patterns of **N-5yTe₆-PEO₃₄** and **N-5yTe₆-PPO₇₄** are shown in Fig. 5a and Fig. 5b, respectively. Both patterns show only broad halos, indicating an amorphous and isotropic structure where **PEO₃** and **PPO₇** do not crystallize. Plots of intensity as a function of 2θ position are also shown in Fig. 5g-i, and these spectra were deconvoluted as described in the Experimental Section. Upon deconvolution, three peaks of **N-5yTe₆-PEO₃₄** can be identified centered at 2θ of 17.3°, 20.8°, and 24.7°, which correspond to d -spacings of 5.12 Å, 4.26 Å, and 3.60 Å, respectively. For **N-5yTe₆-PPO₇₄**, three peaks can be identified centered at 2θ of 17.1°, 20.6° and 25.0°, which corresponds to d -spacings of 5.18 Å, 4.31 Å and 3.55 Å, respectively. These broad halos are attributed to amorphous spacings within the networks.

Next, WAXS was used to investigate the structure of the liquid crystalline networks. All LCN patterns show rings, even for the LC reflections. This is typical of polydomain LC materials, where LC order may be high within a domain but there is no overall ordering of domains so the reflections appear as rings. The WAXS pattern of **N-5yMe₆-PEO₃₄** (Fig. 5c) shows three sharp rings and broad halos. These three rings centered at 2θ of 7.45° ($d_1=11.85$ Å), 9.30° ($d_2=9.50$ Å), and 17.2° ($d_3=5.16$ Å). The sharp ring at 17.2° (5.16 Å) is attributed to spacing between **5yMe** mesogens, which is slightly larger than 4.4-4.5 Å reported previously^{20,68} for methyl-substituted mesogens within a LC network. The rings with d -spacings d_1 and d_2 are suspected to

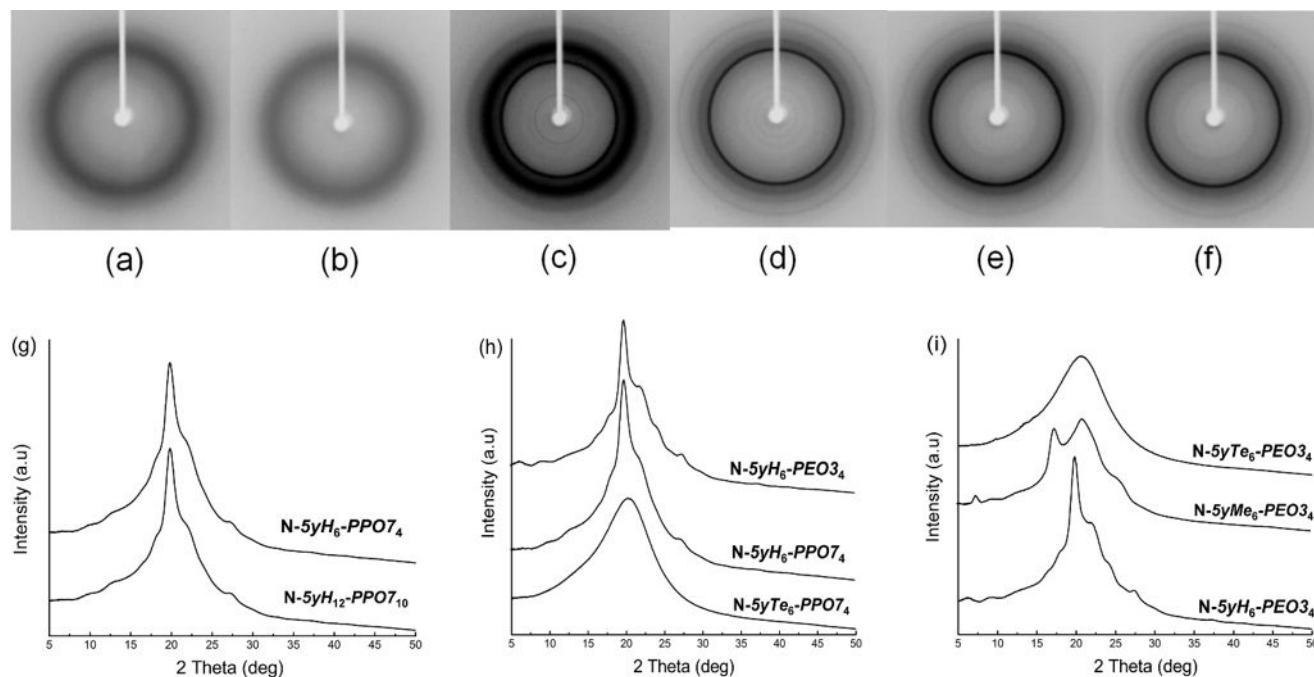


Fig. 5 2D wide angle X-ray scattering of: (a) **N-5yTe₆-PEO₃₄**, (b) **N-5yTe₆-PPO₇₄**, (c) **N-5yMe₆-PEO₃₄**, (d) **N-5yH₆-PEO₃₄**, (e) **N-5yH₆-PPO₇₄**, (f) **N-5yH₁₂-PPO₇₁₀**, and (g-i) Intensity vs 2θ traces obtained from the 2D patterns.

arise from a smectic layer structure. As the broad halos for **5yMe-PEO3** networks are similar to the WAXS pattern of the **5yTe-PEO3** networks, these halos are attributed to amorphous PEO. The WAXS pattern of **N-5yMe₁₂-PEO3₁₀** also shows the same result (data not shown), indicating that the reflections are not changing over this range in crosslink density. For networks containing the **5yH** mesogen, the WAXS pattern of **N-5yH₆-PEO3₄** (Fig. 5d) shows four sharp rings centered at 2θ of 6.50° ($d_1=13.59$ Å), 8.96° ($d_2=9.86$ Å), 19.6° ($d_3=4.53$ Å), and 27.2° ($d_4=3.27$ Å). Both **5yH-PP07** films, **N-5yH₆-PP07₄** (Fig. 5e) and **N-5yH₁₂-PP07₁₀** (Fig. 5f), show four sharp rings centered at 9.71° ($d_1=9.10$ Å), 12.52° ($d_2=7.07$ Å), 19.56° ($d_3=4.52$ Å), and 27.15° ($d_4=3.28$ Å). Because **N-5yH₆-PP07₄**, **N-5yH₁₂-PP07₁₀**, and **N-5yH₆-PEO3₄** each have reflections with d -spacings around 4.52 Å and 3.28 Å, these reflections are thought to originate from spacing between **5yH** mesogens. The other sharp rings with d -spacings around 1 nm are suspected to originate from a reflection associated with the smectic LC phase, but this a subject of current investigation. Finally, the broad halos observed in the **5yH-PEO3** (Fig. 5d) and **5yH-PP07** (Fig. 5d, 5e, and 5f) patterns are attributed to the amorphous PEO and PPO chains within the network.

To investigate longer range ordering in these materials, room temperature small angle X-ray scattering (SAXS) was used. The patterns are shown and described in Supplementary Information (Figure S11). All SAXS patterns of LCNs show one broad halo, located between $q=0.054$ - 0.083 Å⁻¹ ($d=11.57$ - 7.57 nm). These patterns indicating networks display long-range

ordering, but that there is no overall alignment to this structure. This was again expected for the polydomain networks.

SAXS measurements were also conducted at different temperatures (from -10°C to 100°C) to assess how ordering in the LC networks (LCNs) change as a function of temperature. All the tests were run while heating the films at $5^\circ\text{C}/\text{min}$ and holding for 10 minute isothermals at the temperature of interest before acquiring the SAXS measurement. In Fig. 6a for **N-5yMe₆-PEO3₄**, the position and height of SAXS reflection did not change for temperatures under 20°C . Above 20°C , the peak's position moved to lower q and its sharpness increased, as measured by peak width at half-maximum intensity, until the temperature reached 70°C , after which the peak disappeared. For **N-5yH₆-PEO3₄** (Fig. 6b), the peak did not change until heated through 25°C , but loss of the peak was not observed due to the instrument's temperature limit. For **N-5yH₆-PP07₄** (Fig. 6c), the peak become more intense and shifted to lower q once heated above 0°C , and loss of the peak was observed between 90°C and 100°C . For these three LCN compositions, the positions where the SAXS peaks started to sharpen and shift (20°C for **N-5yMe₆-PEO3₄**, 25°C for **N-5yH₆-PEO3₄**, and 0°C for **N-5yH₆-PP07₄**) are consistent the higher temperature end of the first stepwise drop in storage modulus that was observed using DMA. Literature has shown that SAXS reflections of aqueous starch solutions shift to lower q and become sharper upon passing through the glass transition⁸⁴, thus this event, combined with DSC and DMA data, supports that this may be

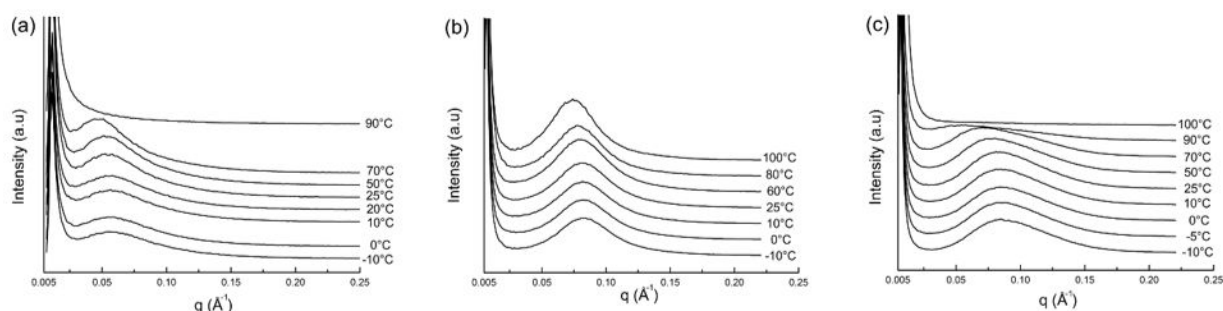


Fig. 6 1D SAXS patterns of (a) **N-5yMe₆-PEO3₄**, (b) **N-5yH₆-PEO3₄**, and (c) **N-5yH₆-PP07₄**. Temperature that each LCN was measured at is noted in the figure.

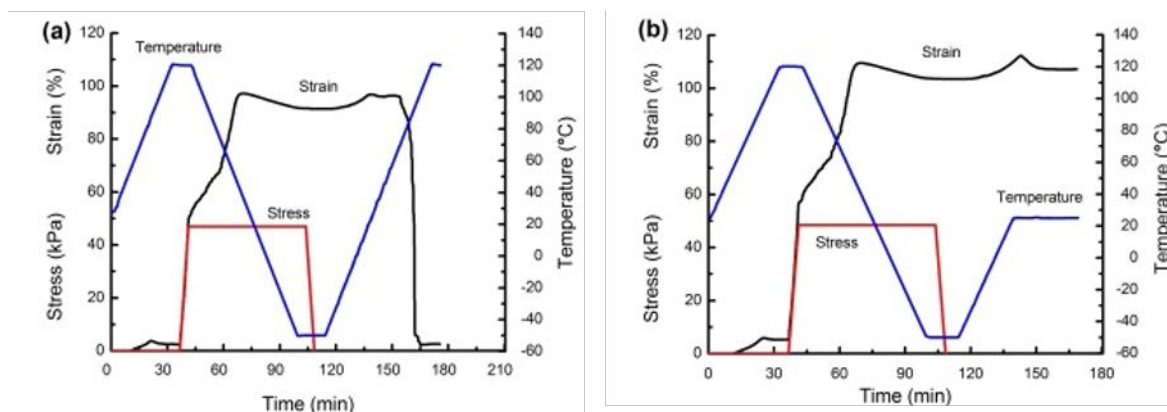


Fig. 7 (a) One-way shape memory with complete recovery of **N-5yH₁₂-PP07₁₀** (b) One-way shape with partial recovery of **N-5yH₁₂-PP07₁₀**.

led to a decrease in chain mobility. For **N-5yMe₆-PEO3₄** and **N-5yH₆-PPO7₄** (Fig 6a and 6c), disappearance of the SAXS reflection occurred at a temperature that was consistent with the isotropization transition observed using DSC and DMA and supports that this is due to loss of LC ordering.

To better understand the type of LC microstructure present in **5yH-PEO3**-based and **PPO7**-based films, WAXS experiments were conducted on strained samples. For WAXS data collection, a mechanical stretching stage could not be used with the instrument employed because it would block the scattered X-rays. As an alternative approach, one-way shape memory (1WSM) was used to deform and fix **5yH** network films in a strained state that was stable for room temperature WAXS experiments. Figure 7a shows a complete one-way shape memory cycle of **N-5yH₁₂-PPO7₁₀**, where the sample could be stretched and fixed at 100% strain and then triggered to completely recover upon heating to the isotropic. A partial 1WSM cycle is shown in Fig. 7b and is representative of the sample preparation method for the strained WAXS experiments. In the partial 1WSM cycle shown, **N-5yH₁₂-PPO7₁₀** was stretched and fixed at 110% before heating back to room temperature and unloading the fixed, elongated specimen from the instrument. Compositions that were stable in the strained state (**5yH**-based networks) were immediately studied with WAXS. Unfortunately, due to the lower transition temperatures of the **5yMe**-based networks, comparable analysis could not be completed without a cooling stage for the X-ray instrument due to the recovery of those compositions at room temperature.

WAXS of two strained networks, both **5yH**-based but one prepared using **PEO3** and the other using **PPO7**, are shown in Fig. 8 (strain axis vertical). **N-5yH₆-PEO3₄** (Fig. 8a,c) was fixed at 60% strain, and **N-5yH₁₂-PPO7₁₀** film was fixed at 140% strain (Fig. 8b,e). Initially, a **N-5yH₆-PPO7₄** film was fixed at 65% strain and analyzed for comparison to **N-5yH₆-PEO3₄** fixed at 60% strain. The reflections of **N-5yH₆-PPO7₄** fixed at 65% strain (see SI Fig. S12, S13) were found to orient in the same direction as **N-5yH₆-PEO3₄** fixed at 60% strain, but the splitting of the reflections was not easily discerned and therefore samples fixed at larger strains were desired for study. Unfortunately, **N-5yH₆-PPO7₄** fixed at double the strain was challenging to accomplish in practice due to its softness. Applying lower stresses to **N-5yH₁₂-PPO7₁₀**, a **5yH-PPO** network with lower crosslink density, was found to permit preparation of the more elongated specimens. Specifically, **N-5yH₁₂-PPO7₁₀** film was fixed at 140% strain and found to orient in the same direction as **N-5yH₆-PPO7₄** fixed at 65% strain as well as to display clearer splitting of reflections. The X-ray data suggests that both **5yH-PPO** and **5yH-PEO** networks form smectic phases. Specifically, the WAXS pattern of stretched **N-5yH₆-PEO3₄** (60% strain) shown in Fig. 8a indicates that the reflection splits into four points at 2θ of 6.50° ($d_1=13.59\text{\AA}$) and 8.96° ($d_2=9.86\text{\AA}$) and 27.2° ($d_3=3.28\text{\AA}$). The WAXS pattern of **N-5yH₁₂-PPO7₁₀** (Fig. 8b) shows four point pattern for the reflections located at 2θ of 9.71° ($d_1=9.01\text{\AA}$) and 12.52° ($d_2=7.06\text{\AA}$). The azimuthal scans are shown in SI for **N-5yH₆-PEO3₄** (Fig. S14) and **N-5yH₁₂-PPO7₁₀** (Fig. S15). This four

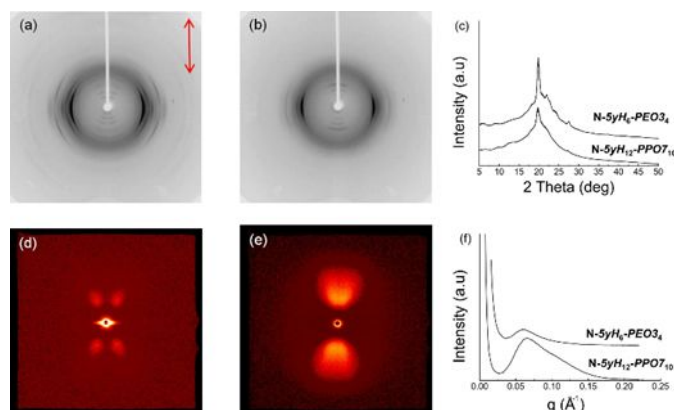


Fig. 8 2D wide-angle X-ray scattering (WAXS) of (a) **N-5yH₆-PEO3₄** (60% strain) and (b) **N-5yH₁₂-PPO7₁₀** (140% strain). (c) 1D WAXS of both networks. 2D small-angle X-ray scattering of (d) **N-5yH₆-PEO3₄** (60% strain) and (e) **N-5yH₁₂-PPO7₁₀** (140% strain). (f) 1D SAXS of both networks. Stretching direction is shown as red arrows in (a).

point splitting pattern suggests that the mesogens order into a smectic-C structure^{85,86}. Other polyether-based LCNs reported in literature form nematic⁷⁹ and smectic⁶⁸ LC phases. For the SAXS patterns, **N-5yH₆-PEO3₄** (Fig. 8d) the reflection at $q=0.061\text{\AA}^{-1}$ ($d=10.3\text{nm}$) splits into four points. The reflection at $q=0.065\text{\AA}^{-1}$ ($d=9.7\text{nm}$) of **N-5yH₁₂-PPO7₁₀** (Fig. 8e) also splits into four parts along the meridian. The splitting is less evident in the **N-5yH₁₂-PPO7₁₀**, but this is attributed to the lower crosslink density which may require stretching to larger strains to orient this material (not possible here due to the travel limit of the instrument). Combining the WAXS and SAXS results, both **N-5yH₆-PEO3₄** and **N-5yH₁₂-PPO7₁₀** are thought to form a smectic-C structure. As described above, this analysis could not be completed on networks based on **5yMe** with **PEO3** and **5yMe** with **PPO7** because of material recovery near room temperature.

This work used copper-catalyzed alkyne-azide cycloaddition to prepare LC networks. While this approach afforded some synthetic benefits compared other synthetic routes to LCNs, most notably slower kinetics and increased tolerance to moisture compared to LCNs synthesized by hydrosilylation, it is recognized that copper is a known antimicrobial and that copper leaching is hazardous to the environment and biological organisms. Additionally, use of these materials in a hydrated form requires them to maintain their LC phases even when hydrated. Previous work has shown that mesogens similar to **5yMe** polymerized with PEO chain extenders form LC phases^{48,68}, but that the LC phase is difficult to detect using conventional DSC and DMA. Torbati and Mather observed that the LC phase of a PEO-based LCN became more evident using X-ray scattering when the networks were hydrated, which was attributed to water promoting phase separation and mesogen association⁶⁸. In this work, the LC phases were strong even in the dry phase, but it was realized that materials could swell and that this could destroy LC organization. Importantly, this was not found, as data showed that LC structures in SAXS were

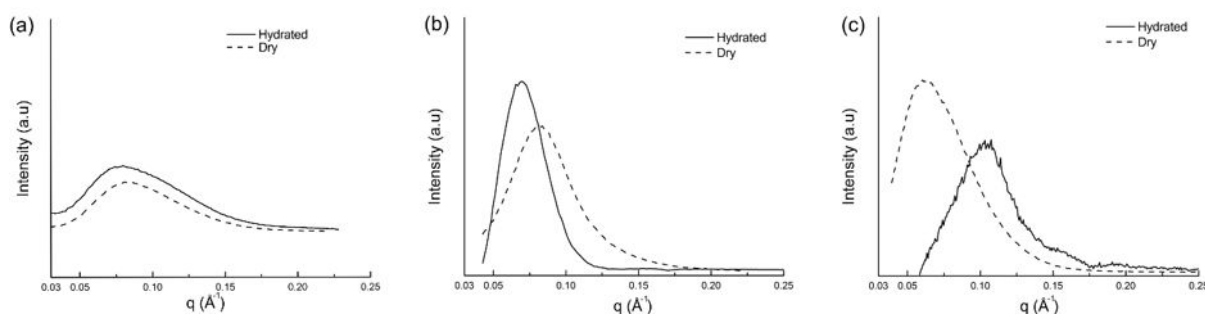


Fig. 9 1D SAXS pattern of hydrated and dry LCNs at 25°C: (a) *N-5yH₆-PPO7₄*, (b) *N-5yH₆-PEO3₄*, and (c) *N-5yH₆-PEO20₄*. All LCNs state showed long-range ordered structure.

stable even in hydrated films (water uptake was 50-150% by weight at room temperature). As examples, 1D-SAXS patterns in the dry and the hydrated states are shown for *N-5yH₆-PPO7₄* (Fig. 9a), *N-5yH₆-PEO3₄* (Fig. 9b), and *N-5yH₆-PEO20₄* (Fig. 9c). The scattering patterns were normalized to sample transmission, and background was subtracted from each using the SAXS software. The position of the peak in hydrated state shifts to lower q for *N-5yH₆-PPO7₄* (Fig. 9a) and *N-5yH₆-PEO3₄* (Fig. 9b) compared to the dry LCN. This result is attributed to water diffusion into the film (*N-5yH₆-PPO7₄* water uptake is 57.1% and *N-5yH₆-PEO3₄* water uptake is 56.8%), which leads to swelling of LC domains and may increase the length scale of phase separation between the more hydrophilic spacer and the more hydrophobic mesogens. *N-5yH₆-PEO20₄* (Fig. 9c) shows the opposite trend, where the hydrated sample shifted to higher q compared to the dry sample. A potential explanation for this behavior is that *N-5yH₆-PEO20₄* has higher water content (148%) due to the larger molecular weight of the PEO chain extender and the resulting lower crosslink density of the network, and that this may drive the mesogens to more closely associate when the network is hydrated to result in a lower q . In each composition, however, the networks maintain a strong LC phase in both hydrated and dry samples, and the tuning of LC phases in hydrated samples is the subject of ongoing investigation.

3.6 Toxicity of the Networks.

To assess initial toxicity of the materials after extraction and copper removal, a Neutral Red assay was performed. The number live cells in contact with different medium was quantified using a standard curve. Medium in which networks were soaked (experimental group), medium incubated with tissue culture plastic (positive control for viability), and medium containing Triton-X 100 (negative control for viability) were compared. Figure 10 shows data normalized to the TCP positive control group, where the normalized cell viability of the networks was 91.1%. One-way ANOVA was used to test statistical difference of the means from the networks, TCP group (positive control for viability), and Triton-X groups (negative control for viability). It was found that both the TCP and the networks displayed statistically significantly higher viability ($p < .0001$) than the Triton-X group, but that there was no statistically significant difference in cell viability between the

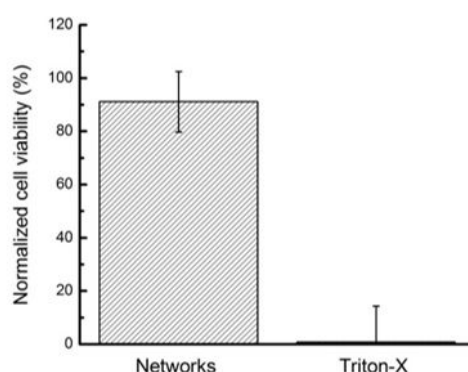


Fig. 10 Human mesenchymal stem cell (hMSC) viability when incubated with medium in contact with networks synthesized by alkyne-azide cycloaddition chemistry for 72 h. Triton-X is negative control for cell viability. All samples are normalized to positive control for viability, which was medium incubated with tissue culture polystyrene plates.

Click chemistry networks and the tissue culture plastic. Importantly, this data indicates that any extractable materials from the purified networks are not toxic towards the cells, but more extensive biocompatibility tests are ongoing.

4. Conclusions

We have reported the synthesis of PEO and PPO-based main-chain liquid crystalline networks using copper-catalyzed "Click" chemistry. Microstructure and thermomechanical properties were characterized by DSC, DMA, and X-ray scattering. The polyether spacers selected for study were lower in molecular weight (PEO) and/or different in composition (PPO) than other polyether spacers previously reported for LCNs, as this was anticipated to reduce the likelihood that the spacer would crystallize and disrupt LC phase formation. For all compositions investigated, spacer crystallization was not observed, and no difference in toxicity towards human mesenchymal stem cells was observed relative to tissue culture plastic.

Networks synthesized using the *5yH* mesogen formed LC phases for all polyether spacers studied, but *5yMe*-based networks only formed LC phases when the shortest PEO spacer was used. The strength of the LC phase in the *5yH*-based

networks is evidenced by the ability to detect isotropization using both differential scanning calorimetry and dynamic mechanical analysis, a feature not present in the **SyMe**-based networks reported here and by others. For **SyH-PEO** and **SyH-PPO** networks, X-ray scattering of strained samples fixed using one way-shape memory revealed that the networks form smectic phases. However, it is not clear if the **SyMe**-based networks that form LC phases are also smectic due to instrument limitations. All **SyH** LC networks undergo reversible thermomechanical actuation (two-way shape memory) associated with the order-disorder transition of the networks. In contrast, **SyMe**-based networks underwent thermomechanical actuation around temperatures that are closer to the crystallization temperature of PEO. This suggests that order-disorder changes under strain in some compositions of **SyMe** networks may also be accompanied with PEO crystallization, but it is noted that this would need to be investigated using X-ray scattering coupled with heating and cooling under strain. Importantly, the strong LC phases present in the materials reported result in stable LC phases both in the dry and hydrated states. Combining the strong LC phases with low cytotoxicity in these networks is expected to enable their use as hydrated and responsive substrates for environmental and biological applications.

Conflicts of interest

There are no conflicts to declare.

Acknowledgements

The authors wish to thank the University of Connecticut for supporting this work through the Research Excellence Program and Burke Laboratory start-up funds. Small and Wide Angle X-ray data was collected on a Bruker NANOSTAR that was acquired through a Major Research Instrumentation award from National Science Foundation (DMR 1228817). The authors also wish to thank Dr. Kuo-Chih Shih (Department of Agricultural Chemistry, National Taiwan University, Taipei, Taiwan, R. O. C.) and Prof. Mu-Ping Nieh (Chemical and Biomolecular Engineering and Polymer Program, University of Connecticut, Storrs, CT USA) for insightful discussions and assistance interpreting small angle X-ray scattering data. Finally, the authors wish to thank Prof. David Kaplan, Biomedical Engineering, Tufts University for the generous gift of a vial of human mesenchymal stem cells.

References

- (1) Warner, M.; Terentjev, E. M. *Liquid Crystal Elastomers*; Oxford University Press: New York, 2003.
- (2) *Cross-Linked Liquid Crystalline Systems: From Rigid Polymer Networks to Elastomers*; Broer, D. J., Crawford, G. P., Zumer, S., Eds.; CRC Press: New York, 2011.
- (3) *Liquid Crystal Elastomers: Materials and Applications*; de Jeu, W. H., Ed.; Springer: New York, 2012.
- (4) Zhao, F.; Bi, W.; Zhao, S. Influence of Crosslink Density on Mechanical Properties of Natural Rubber Vulcanizates. *J. Macromol. Sci. Part B Phys.* **2011**, *50* (7), 1460–1469.
- (5) White, T. J.; Broer, D. J. Programmable and Adaptive Mechanics with Liquid Crystal Polymer Networks and Elastomers. *Nat. Mater.* **2015**, *14* (11), 1087–1098.
- (6) Wertmer, H.; Finkelmann, H. Liquid Crystalline Elastomers as Artificial Muscles. *e-Polymers* **2001**, *013*, 1–13.
- (7) Thomsen, D. L.; Keller, P.; Naciri, J.; Pink, R.; Jeon, H.; Shenoy, D.; Ratna, B. R. Liquid Crystal Elastomers with Mechanical Properties of a Muscle. *Macromolecules* **2001**, *34* (17), 5868–5875.
- (8) Finkelmann, H.; Kim, S. T.; Muñoz, A.; Palffy-Muhoray, P.; Taheri, B. Tunable Mirrorless Lasing in Cholesteric Liquid Crystalline Elastomers. *Adv. Mater.* **2001**, *13* (14), 1069–1072.
- (9) Ren, H.; Wu, S. T. Tunable Electronic Lens Using a Gradient Polymer Network Liquid Crystal. *Appl. Phys. Lett.* **2003**, *82* (1), 22–24.
- (10) Xie, P.; Zhang, R. Liquid Crystal Elastomers, Networks and Gels: Advanced Smart Materials. *J. Mater. Chem.* **2005**, *15* (26), 2529.
- (11) de Gennes, P. G. Reflexions Sur Un Type de Polymeres Nematiques. *Comptes rendus l'Académie des Sci.* **1975**, *281*, 101–103.
- (12) Spillmann, C. M.; Naciri, J.; Chen, M.-S.; Srinivasan, A.; Ratna, B. R. Tuning the Physical Properties of a Nematic Liquid Crystal Elastomer Actuator. *Liq. Cryst.* **2006**, *33* (4), 373–380.
- (13) Küpfer, J.; Nishikawa, E.; Finkelmann, H. Densely Crosslinked Liquid Single-crystal Elastomers. *Polym. Adv. Technol.* **1994**, *5* (2), 110–115.
- (14) Naciri, J.; Srinivasan, A.; Jeon, H.; Nikolov, N.; Keller, P.; Ratna, B. R. Nematic Elastomer Fiber Actuator. *Macromolecules* **2003**, *36* (22), 8499–8505.
- (15) Donnio, B.; Wermter, H.; Finkelmann, H. A Simple and Versatile Synthetic Route for the Preparation of Main-Chain, Liquid-Crystalline Elastomers. *Macromolecules* **2000**, *33* (21), 7724–7729.
- (16) Bergmann, G. H. F.; Finkelmann, H.; Percec, V.; Zhao, M. Liquid-Crystalline Main-Chain Elastomers. *Macromol. Rapid Commun.* **1997**, *18* (5), 353–360.
- (17) Wermter, H.; Finkelmann, H. Liquid Crystalline Elastomers as Artificial Muscles. *e-Polymers* **2001**, *1* (1), 013.
- (18) Tokita, M.; Tagawa, H.; Ishige, R.; Osada, K.; Watanabe, J. Thermally Reversible Distortion Observed for Monodomain Nematic Elastomer of Cross-Linked Main-Chain Polyester. *Mol. Cryst. Liq. Cryst.* **2007**, *465* (1), 193–202.
- (19) Amela-Cortés, M.; Bruce, D. W.; Evans, K. E.; Smith, C. W. Unsymmetric Main-Chain Liquid Crystal Elastomers with Tunable Phase Behaviour: Elastic Response. *J. Mater. Chem.* **2011**, *21* (23), 8436–8442.
- (20) Burke, K. A.; Rousseau, I. A.; Mather, P. T. Reversible Actuation in Main-Chain Liquid Crystalline Elastomers with Varying Crosslink Densities. *Polym. (United Kingdom)* **2014**, *55* (23), 5897–5907.
- (21) Sanchez-Ferrer, A.; Finkelmann, H. Thermal and

- Mechanical Properties of New Main-Chain Liquid Crystalline Elastomers. *Mol. Cryst. Liq. Cryst.* **2009**, *508*, 348–356.
- (22) Burke, K. A.; Mather, P. T. Soft Shape Memory in Main-Chain Liquid Crystalline Elastomers. *J. Mater. Chem.* **2010**, *20*, 3449–3457.
- (23) Yu, Y.; Nakano, M.; Shishido, A.; Shiono, T.; Ikeda, T. Effect of Cross-Linking Density on Photoinduced Bending Behavior of Oriented Liquid-Crystalline Network Films Containing Azobenzene. *Chem. Mater.* **2004**, *16* (9), 1637–1643.
- (24) Lee, K.; Koerner, H.; Vaia, R.; Bunning, T.; White, T. Relationship between the Photomechanical Response and the Thermomechanical Properties of Azobenzene Liquid Crystalline Polymer Networks. *Macromolecules* **2010**, *43*, 8185–8190.
- (25) Van Oosten, C. L.; Bastiaansen, C. W. M.; Broer, D. J. Printed Artificial Cilia from Liquid-Crystal Network Actuators Modularly Driven by Light. *Nat. Mater.* **2009**, *8* (8), 677–682.
- (26) Schuhladen, S.; Preller, F.; Rix, R.; Petsch, S.; Zentel, R.; Zappe, H. Iris-like Tunable Aperture Employing Liquid-Crystal Elastomers. *Adv. Mater.* **2014**, *26* (42), 7247–7251.
- (27) Agrawal, A.; Luchette, P.; Palfy-Muhoray, P.; Biswal, S. L.; Chapman, W. G.; Verduzco, R. Surface Wrinkling in Liquid Crystal Elastomers. *Soft Matter* **2012**, *8* (27), 7138.
- (28) Pei, Z.; Yang, Y.; Chen, Q.; Terentjev, E. M.; Wei, Y.; Ji, Y. Mouldable Liquid-Crystalline Elastomer Actuators with Exchangeable Covalent Bonds. *Nat. Mater.* **2014**, *13* (1), 36–41.
- (29) Torras, N.; Zinoviev, K. E.; Esteve, J.; Sánchez-Ferrer, A. Liquid-Crystalline Elastomer Micropillar Array for Haptic Actuation. *J. Mater. Chem. C* **2013**, *1* (34), 5183.
- (30) Kohlmeyer, R. R.; Chen, J. Wavelength-Selective, IR Light-Driven Hinges Based on Liquid Crystalline Elastomer Composites. *Angew. Chemie - Int. Ed.* **2013**, *52* (35), 9234–9237.
- (31) Camargo, C. J.; Campanella, H.; Marshall, J. E.; Torras, N.; Zinoviev, K.; Terentjev, E. M.; Esteve, J. Localised Actuation in Composites Containing Carbon Nanotubes and Liquid Crystalline Elastomers. *Macromol. Rapid Commun.* **2011**, *32* (24), 1953–1959.
- (32) Haberl, J. M.; Sanchez-Ferrer, A.; Mihut, A. M.; Dietsch, H.; Hirt, A. M.; Mezzenga, R. Liquid-Crystalline Elastomer-Nanoparticle Hybrids with Reversible Switch of Magnetic Memory. *Adv. Mater.* **2013**, *25* (12), 1787–1791.
- (33) Ware, T. H.; McConney, M. E.; Wie, J. J.; Tondiglia, V. P.; White, T. J. Voxellated Liquid Crystal Elastomers. *Science (80-.)* **2015**, *347* (6225), 982–984.
- (34) Finkelmann, H.; Kock, H.; Rehage, G. Investigations on Liquid Crystalline Polysiloxanes 3. Liquid Crystalline Elastomers -- a New Type of Liquid Crystalline Material. *Die Makromol. Chemie, Rapid Commun.* **1981**, *2*, 317–322.
- (35) Seki, T.; Nagano, S.; Hara, M. Versatility of Photoalignment Techniques: From Nematics to a Wide Range of Functional Materials. *Polym. (United Kingdom)* **2013**, *54*, 6053–6072.
- (36) Hoyle, C. E.; Watanabe, T.; Whitehead, J. B. Anisotropic Network Formation by Photopolymerization of Liquid Crystal Monomers in a Low Magnetic Field. *Macromolecules* **1994**, *27* (22), 6581–6588.
- (37) Sanchez-Ferrer, A.; Fischl, T.; Stubenrauch, M.; Albrecht, A.; Wurmus, H.; Hoffmann, M.; Finkelmann, H. Liquid-Crystalline Elastomer Microvalve for Microfluidics. *Adv. Mater.* **2011**, *23* (39), 4526–4530.
- (38) Shenoy, D. K.; Laurence Thomsen Iii, D.; Srinivasan, A.; Keller, P.; Ratna, B. R. Carbon Coated Liquid Crystal Elastomer Film for Artificial Muscle Applications. *Sensors Actuators, A Phys.* **2002**, *96* (2–3), 184–188.
- (39) Li, M.; Keller, P. Artificial Muscles Based on Liquid Crystal Elastomers. *Philos. Trans. A* **2006**, *364*, 2763–2777.
- (40) Camacho-Lopez, M.; Finkelmann, H.; Palfy-Muhoray, P.; Shelley, M. Fast Liquid-Crystal Elastomer Swims into the Dark. *Nat. Mater.* **2004**, *3*, 307–310.
- (41) Yamada, M.; Kondo, M.; Miyasato, R.; Naka, Y.; Mamiya, J.-I.; Kinoshita, M.; Shishido, A.; Yu, Y.; Barrett, C. J.; Ikeda, T. Photomobile Polymer Materials - Various Three-Dimensional Movements. *J. Mater. Chem.* **2009**, *19* (1), 60–62.
- (42) Zeng, H.; Wasylczyk, P.; Cerretti, G.; Martella, D.; Parmeggiani, C.; Wiersma, D. S. Alignment Engineering in Liquid Crystalline Elastomers: Free-Form Microstructures with Multiple Functionalities. *Appl. Phys. Lett.* **2015**, *106* (11).
- (43) Zeng, H.; Wasylczyk, P.; Parmeggiani, C.; Martella, D.; Burreli, M.; Wiersma, D. S. Light-Fueled Microscopic Walkers. *Adv. Mater.* **2015**, *27* (26), 3883–3887.
- (44) Martella, D.; Nocentini, S.; Nuzhdin, D.; Parmeggiani, C.; Wiersma, D. S. Photonic Microhand with Autonomous Action. *Adv. Mater.* **2017**, *29* (42).
- (45) Agrawal, A.; Chen, H.; Kim, H.; Zhu, B.; Adetiba, O.; Miranda, A.; Cristian Chipara, A.; Ajayan, P. M.; Jacot, J. G.; Verduzco, R. Electromechanically Responsive Liquid Crystal Elastomer Nanocomposites for Active Cell Culture. *ACS Macro Lett.* **2016**, *5* (12), 1386–1390.
- (46) Sharma, A.; Neshat, A.; Mahnen, C. J.; Nielsen, A. D.; Snyder, J.; Stankovich, T. L.; Daum, B. G.; Laspina, E. M.; Beltrano, G.; Gao, Y.; et al. Biocompatible, Biodegradable and Porous Liquid Crystal Elastomer Scaffolds for Spatial Cell Cultures. *Macromol. Biosci.* **2015**, *15*, 200–214.
- (47) Agrawal, A.; Adetiba, O.; Kim, H.; Chen, H.; Jacot, J. G.; Verduzco, R. Stimuli-Responsive Liquid Crystal Elastomers for Dynamic Cell Culture. *J. Mater. Res.* **2015**, *30* (4), 453–462.
- (48) Yakacki, C. M.; Saed, M.; Nair, D. P.; Gong, T.; Reed, S. M.; Bowman, C. N. Tailorable and Programmable Liquid-Crystalline Elastomers Using a Two-Stage Thiol-acrylate Reaction. *RSC Adv.* **2015**, *5* (25), 18997–19001.
- (49) Prévôt, M. E.; Andro, H.; Alexander, S. L. M.; Ustunel, S.; Zhu, C.; Nikolov, Z.; Rafferty, S. T.; Brannum, M. T.; Kinsel, B.; Korley, L. T. J.; et al. Liquid Crystal Elastomer Foams with Elastic Properties Specifically Engineered as Biodegradable Brain Tissue Scaffolds. *Soft Matter* **2018**, *14* (3), 354–360.
- (50) Gao, Y.; Mori, T.; Manning, S.; Zhao, Y.; Nielsen, A. D.;

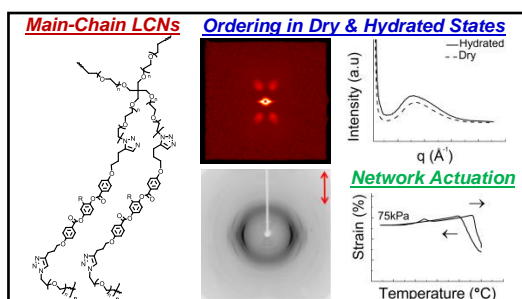
- Neshat, A.; Sharma, A.; Mahnen, C. J.; Everson, H. R.; Crotty, S.; et al. Biocompatible 3D Liquid Crystal Elastomer Cell Scaffolds and Foams with Primary and Secondary Porous Architecture. *ACS Macro Lett.* **2016**, *5* (1), 4–9.
- (51) Bera, T.; Freeman, E. J.; McDonough, J. A.; Clements, R. J.; Aladlaan, A.; Miller, D. W.; Malcuit, C.; Hegmann, T.; Hegmann, E. Liquid Crystal Elastomer Microspheres as Three-Dimensional Cell Scaffolds Supporting the Attachment and Proliferation of Myoblasts. *ACS Appl. Mater. Interfaces* **2015**, *7* (26), 14528–14535.
- (52) Martella, D.; Paoli, P.; Pioner, J. M.; Sacconi, L.; Coppini, R.; Santini, L.; Lulli, M.; Cerbai, E.; Wiersma, D. S.; Poggesi, C.; et al. Liquid Crystalline Networks toward Regenerative Medicine and Tissue Repair. *Small* **2017**, *13* (46).
- (53) Ponniah, J. K.; Chen, H.; Adetiba, O.; Verduzco, R.; Jacot, J. G. Mechanoactive Materials in Cardiac Science. *J. Mater. Chem. B* **2016**, *4* (46), 7350–7362.
- (54) Koçer, G.; ter Schiphorst, J.; Hendriks, M.; Kassa, H. G.; Leclère, P.; Schenning, A. P. H. J.; Jonkheijm, P. Light-Responsive Hierarchically Structured Liquid Crystal Polymer Networks for Harnessing Cell Adhesion and Migration. *Adv. Mater.* **2017**, *29* (27).
- (55) Prévôt, M. E.; Ustunel, S.; Hegmann, E. Liquid Crystal Elastomers-A Path to Biocompatible and Biodegradable 3D-LCE Scaffolds for Tissue Regeneration. *Materials (Basel)*. **2018**, *11* (3).
- (56) Hoyle, C. E.; Bowman, C. N. Thiol-Ene Click Chemistry. *Angew. Chemie - Int. Ed.* **2010**, *49* (9), 1540–1573.
- (57) Hong, Y.; Buguin, A.; Taulemesse, J.-M.; Kaneko, K.; Méry, S.; Bergeret, A.; Keller, P. Micron-Sized Main-Chain Liquid Crystalline Elastomer Actuators with Ultralarge Amplitude Contractions. *J. Am. Chem. Soc.* **2009**, *131* (41), 15000–15004.
- (58) Fleischmann, E.-K.; Forst, F. R.; Köder, K.; Kapernaum, N.; Zentel, R. Microactuators from a Main-Chain Liquid Crystalline Elastomer via Thiol-Ene “Click” Chemistry. *J. Mater. Chem. C* **2013**, *1* (37), 5885–5891.
- (59) Campos, L. M.; Meinel, I.; Guino, R. G.; Schierhorn, M.; Gupta, N.; Stucky, G. D.; Hawker, C. J. Highly Versatile and Robust Materials for Soft Imprint Lithography Based on Thiol-Ene Click Chemistry. *Adv. Mater.* **2008**, *20* (19), 3728–3733.
- (60) Polizzotti, B. D.; Fairbanks, B. D.; Anseth, K. S. Three-Dimensional Biochemical Patterning of Click-Based Composite Hydrogels via Thiolene Photopolymerization. *Biomacromolecules* **2008**, *9* (4), 1084–1087.
- (61) Bryant, S. J.; Nuttelman, C. R.; Anseth, K. S. Cytocompatibility of UV and Visible Light Photoinitiating Systems on Cultured NIH/3T3 Fibroblasts in Vitro. *J. Biomater. Sci. Polym. Ed.* **2000**, *11* (5), 439–457.
- (62) Meldal, M.; Tomøe, C. W. Cu-Catalyzed Azide - Alkyne Cycloaddition. *Chem. Rev.* **2008**, *108* (8), 2952–3015.
- (63) Binder, W. H.; Sachsenhofer, R. “Click” Chemistry in Polymer and Material Science: An Update. *Macromol. Rapid Commun.* **2008**, *29* (12–13), 952–981.
- (64) Chang, P. V.; Prescher, J. A.; Sletten, E. M.; Baskin, J. M.; Miller, I. A.; Agard, N. J.; Lo, A.; Bertozzi, C. R. Copper-Free Click Chemistry in Living Animals. *Proc. Natl. Acad. Sci. U. S. A.* **2010**, *107* (5), 1821–1826.
- (65) Jewett, J. C.; Sletten, E. M.; Bertozzi, C. R. Rapid Cu-Free Click Chemistry with Readily Synthesized Biarylazacyclooctynones. *J. Am. Chem. Soc.* **2010**, *132* (11), 3688–3690.
- (66) Johnson, J. A.; Baskin, J. M.; Bertozzi, C. R.; Koberstein, J. T.; Turro, N. J. Copper-Free Click Chemistry for the in Situ Crosslinking of Photodegradable Star Polymers. *Chem. Commun.* **2008**, No. 26, 3064–3066.
- (67) Seo, T. S.; Li, Z.; Ruparel, H.; Ju, J. Click Chemistry to Construct Fluorescent Oligonucleotides for DNA Sequencing. *J. Org. Chem.* **2003**, *68* (2), 609–612.
- (68) Torbati, A. H.; Mather, P. T. A Hydrogel-Forming Liquid Crystalline Elastomer Exhibiting Soft Shape Memory. *J. Polym. Sci. Part B Polym. Phys.* **2016**, *54* (1), 38–52.
- (69) Rousseau, I. A.; Qin, H.; Mather, P. T. Tailored Phase Transitions via Mixed Mesogen Liquid Crystalline Polymers with Silicon-Based Spacers. *Macromolecules* **2005**, *38*, 4103–4113.
- (70) Arehart, S. V. V.; Pugh, C. Induction of Smectic Layering in Nematic Liquid Crystals Using Immiscible Components. 1. Laterally Attached Side-Chain Liquid Crystalline Poly(Norbornene)s and Their Low Molar Mass Analogs with Hydrocarbon/Fluorocarbon Substituents. *J. Am. Chem. Soc.* **1997**, *119* (13), 3027–3037.
- (71) Burke, K. A.; Mather, P. T. Crosslinkable Liquid Crystalline Copolymers with Variable Isotropization Temperature. *J. Mater. Chem.* **2012**, *22*, 14518–14530.
- (72) Patton, J. T.; Boncella, J. M.; Wagener, K. B. Acyclic Diene Metathesis (ADMET) Polymerization. The Synthesis of Unsaturated Polyesters. *Macromolecules* **1992**, *25* (15), 3862–3867.
- (73) June, S. M.; Bissel, P.; Long, T. E. Segmented Block Copolyesters Using Click Chemistry. *J. Polym. Sci. Part A Polym. Chem.* **2012**, *50* (18), 3797–3805.
- (74) Repetto, G.; del Peso, A.; Zurita, J. L. Neutral Red Uptake Assay for the Estimation of Cell Viability/ Cytotoxicity. *Nat. Protoc.* **2008**, *3* (7), 1125–1131.
- (75) Jackson Jr., W. J. Liquid Crystal Polymers: VI. Liquid Crystalline Polyesters of Substituted Hydroquinones. In *Contemporary Topics in Polymer Science*; 1984; Vol. 5, pp 177–208.
- (76) Heitz, W.; Neibner, N. Synthesis and Characterization of Substituted Aromatic Polyesters Derived from Phenoxy- and Tert-Butylhydroquinone. *Makromol. Chemie* **1990**, *191*, 225–235.
- (77) Bhowmik, P. K.; Han, H. Fully Aromatic Liquid Crystalline Polyesters of Phenyl-Substituted 4,4'-Biphenols and 1,1'-Binaphthyl-4,4'-Diol and Either 2-Bromoterephthalic Acid or 2-Phenylterephthalic Acid. *Macromolecules* **1993**, *26*, 5287–5294.
- (78) Gaudiana, R. A.; Minns, R. A.; Sinta, R.; Weeks, N.; Rogers, H. G. Amorphous Rigid-Rod Polymers. *Prog. Polym. Sci.* **1989**, *14*, 47–89.
- (79) Saed, M. O.; Torbati, A. H.; Starr, C. A.; Visvanathan, R.; Clark, N. A.; Yakacki, C. M. Thiol-Acrylate Main-Chain

- Liquid-Crystalline Elastomers with Tunable Thermomechanical Properties and Actuation Strain. *J. Polym. Sci. Part B Polym. Phys.* **2017**, *55* (2), 157–168.
- (80) Majumdar, R.; Alexander, K. S.; Riga, A. T. Physical Characterization of Polyethylene Glycols by Thermal Analytical Technique and the Effect of Humidity and Molecular Weight. *Pharmazie* **2010**, *65* (5), 342–346.
- (81) Li, J.; Rodgers, W. R.; Xie, T. Semi-Crystalline Two-Way Shape Memory Elastomer. *Polymer (Guildf)*. **2011**, *52* (23), 5320–5325.
- (82) Chung, T.; Romo-Uribe, A.; Mather, P. T. Two-Way Reversible Shape Memory in a Semicrystalline Network. *Macromolecules* **2008**, *41*, 184–192.
- (83) Ohm, C.; Brehmer, M.; Zentel, R. Liquid Crystalline Elastomers as Actuators and Sensors. *Adv. Mater.* **2010**, *22* (31), 3366–3387.
- (84) Waigh, T. A.; Perry, P.; Riekkel, C.; Gidley, M. J.; Donald, A. M. Chiral Side-Chain Liquid-Crystalline Polymeric Properties of Starch. *Macromolecules* **1998**, *31* (22), 7980–7984.
- (85) Dey, S.; Agra-Kooijman, D. M.; Ren, W.; McMullan, P. J.; Griffin, A. C.; Kumar, S. Soft Elasticity in Main Chain Liquid Crystal Elastomers. *Crystals* **2013**, *3* (2), 363–390.
- (86) Burke, K. A.; Mather, P. T. Evolution of Microstructure during Shape Memory Cycling of a Main-Chain Liquid Crystalline Elastomer. *Polymer (Guildf)*. **2013**, *54*, 2808–2820.

Table of Contents Figure for

Phase behavior of main-chain liquid crystalline polymer
networks synthesized by alkyne-azide cycloaddition
chemistry

Yongjian Wang^a and Kelly A. Burke^{a,b,c*}



Tuning composition of main-chain liquid crystalline “Click” networks reveals long range order, even when hydrated, and shape morphing behaviors.